Transition to instability in a periodically kicked Bose-Einstein condensate on a ring

Jie Liu,[1,2,*] Chuanwei Zhang,[2,3,*] Mark G. Raizen,[2,3] and Qian Niu[2]
[1]*Institute of Applied Physics and Computational Mathematics, Beijing 100088, People's Republic of China*
[2]*Department of Physics, The University of Texas, Austin, Texas 78712-1081, USA*
[3]*Center for Nonlinear Dynamics, The University of Texas, Austin, Texas 78712-1081, USA*
(Received 29 August 2005; published 3 January 2006)

A periodically kicked ring of a Bose-Einstein condensate is considered as a nonlinear generalization of the quantum kicked rotor, where the nonlinearity stems from the mean-field interactions between the condensed atoms. For weak interactions, periodic motion (antiresonance) becomes quasiperiodic (quantum beating) but remains stable. There exists a critical strength of interactions beyond which quasiperiodic motion becomes chaotic, resulting in an instability of the condensate manifested by exponential growth in the number of noncondensed atoms. In the stable regime, the system remains predominantly in the two lowest energy states and may be mapped onto a spin model, from which we obtain an analytic expression for the beat frequency and discuss the route to instability. We numerically explore a parameter regime for the occurrence of instability and reveal the characteristic density profile for both condensed and noncondensed atoms. The Arnold diffusion to higher energy levels is found to be responsible for the transition to instability. Similar behavior is observed for dynamically localized states (essentially quasiperiodic motions), where stability remains for weak interactions but is destroyed by strong interactions.

DOI: 10.1103/PhysRevA.73.013601 PACS number(s): 03.75.Kk, 05.45.−a, 42.50.Vk

I. INTRODUCTION

The δ-kicked rotor is a textbook paradigm for the study of classical and quantum chaos [1]. In the classical regime, increasing kick strengths destroy regular periodic or quasiperiodic motions of the rotor and lead to the transition to chaotic motions, characterized by diffusive growth in the kinetic energy. In quantum mechanics, chaos is no longer possible because of the linearity of the Schrödinger equation and the motion becomes periodic (anti-resonance), quasiperiodic (dynamical localization), or resonant (quantum resonance) [2,3]. Experimental study of these quantum phenomena have been done with ultracold atoms in periodically pulsed optical lattices [4]. However, most of the previous investigations have been focused on single-particle systems and the effects of interaction between particles have not received much attention [5,6].

In recent years, the realization of Bose-Einstein condensation (BEC) [7] of dilute gases has opened interesting opportunities for studying dynamical systems in the presence of many-body interactions. One cannot only prepare initial states with unprecedented precision and pureness, but one also has the freedom of introducing interactions between the particles in a controlled manner. A natural question to ask is how the physics of the quantum kicked rotor is modified by the interactions. In the mean-field approximation, many-body interactions in BEC are represented by adding a nonlinear term in the Schrödinger equation [8] (such a nonlinear Schrödinger equation also appears in the context of nonlinear optics [9]). This nonlinearity makes it possible to bring chaos back into the system, leading to instability (in the sense of exponential sensitivity to initial conditions) of the condensate wave function [10]. The onset of instability of the condensate can cause rapid proliferation of thermal particles [11] that can be observed in experiments [12]. It is therefore important to understand the route to chaos with increasing interactions. This problem has recently been studied for the kicked BEC in a harmonic oscillator [6].

In Ref. [13], we have investigated the quantum dynamics of a BEC with repulsive interaction that is confined on a ring and kicked periodically. This system is a nonlinear generalization of the quantum kicked rotor. From the point of view of dynamical theory, the kicked rotor is more generic than the kicked harmonic oscillator, because it is a typical low dimensional system that obeys the KAM theorem, while the kicked harmonic oscillator is known to be a special degenerate system out of the framework of the KAM theorem [14]. It is very interesting to understand how both quantum mechanics and mean-field interaction affect the dynamics of such a generic system.

In this paper, we extend the results of Ref. [13], including a more detailed analysis of the model considered there as well as different phenonmena. We will focus our attention on the relatively simpler case of quantum antiresonance, and show how the state is driven towards chaos or instability by the mean-field interaction. The paper is orgnaized as follows: Section II lays out our physical model and its experimental realization. Section III is devoted to the case of weak interactions between atoms. We find that weak interactions make the periodic motion (antiresonance) quasiperiodic in the form of quantum beating. However, the system remains predominantly in the lowest two energy levels and analytic expressions for the beating frequencies are obtained by mapping the system onto a spin model. Through varying the kick period, we find that the phenomenon of antiresonance may be recovered even in the presence of interactions. The decoherence effects due to thermal noise are discussed. Section IV is devoted to the case of strong interactions. It is found that

*These authors contributed equally to this work.

there exists a critical strength of interactions beyond which quasiperiodic motion (quantum beating) is destroyed, resulting in a transition to instability of the condensate characterized by an exponential growth in the number of noncondensed atoms. Universal critical behavior for the transition is found. We show that the occurrence of instability corresponds to the process of Arnold diffusion, through which the state can penetrate through the KAM tori and escape to high-energy levels [15]. We study nonlinear effects on dynamically localized states that may be regarded as quasiperiodic [16]. Similar results are obtained in that localization remians for sufficiently weak interactions but become unstable beyond a critical strength of interactions. Section V consists of conclusions.

II. PHYSICAL MODEL: KICKED BEC ON A RING

Although the results obtained in this paper are common properties of systems whose dynamics are governed by the nonlinear Schrödinger equation, we choose to present them here for a concrete physical model: a kicked BEC confined on a ring trap, where the physical meanings of the results are easy to understand. The description of the dynamics of this system may be divided into two parts: condensed atoms and noncondensed atoms.

A. Dynamics of condensed atoms: Gross-Pitaevskii equation

Consider condensed atoms confined in a toroidal trap of radius R and thickness r, where $r \ll R$ so that lateral motion is negligible and the system is essentially one-dimensional [17]. The dynamics of the BEC is described by the dimensionless nonlinear Gross-Pitaveskii (GP) equation,

$$i\frac{\partial}{\partial t}\psi = \left(-\frac{1}{2}\frac{\partial^2}{\partial\theta^2} + g|\psi|^2 + K(\cos\theta)\delta_t(T)\right)\psi, \tag{1}$$

where $g=8NaR/r^2$ is the scaled strength of nonlinear interaction, N is the number of atoms, a is the s-wave scattering length, K is the kick strength, $\delta_t(T)$ represents $\Sigma_n\delta(t-nT)$, T is the kick period, and θ denotes the azimuthal angle. The length and the energy are measured in units R and $\hbar^2/mR^2$, respectively. The wave function $\psi(\theta,t)$ has the normalization $\int_0^{2\pi}|\psi|^2 d\theta=1$ and satisfies periodic boundary condition $\psi(\theta,t)=\psi(\theta+2\pi,t)$.

Experimentally, the ring-shape potential may be realized using two two-dimensional (2D) circular "optical billiards" with the lateral dimension being confined by two plane optical billiards [18], or optical-dipole traps produced by red-detuned Laguerre-Gaussian laser beams of varying azimuthal mode index [19]. The δ kick may be realized by adding potential points along the ring with an off-resonant laser [4], or by illuminating the BEC with a periodically pulsed strongly detuned running wave laser in the lateral direction whose intensity I is engineered to $I=I_0+I_1x/R$ [20]. In the experiment, we have the freedom to replace the periodic modulation $\cos(\theta)$ of the kick potential with $\cos(j\theta)$, where j is an integer. Such replacement revises the scaled interaction constant g and kicked strength K, but will not affect the results obtained in the paper. The interaction strength g may be adjusted using a magnetic-field-dependent Feshbach resonance or the variation of the number of atoms [21].

B. Dynamics of noncondensed atoms: Bogoliubov equation

The deviation from the condensate wave function is described by Bogoliubov equation that is obtained from a linearization around the GP equation [11]. In Castin and Dum's formalism, the mean number of noncondensed atoms at zero temperature is described by $\langle\delta\hat{N}(t)\rangle=\Sigma_{k=1}^{\infty}\langle v_k(t)|v_k(t)\rangle$, where $v_k(t)$ are governed by

$$i\frac{d}{dt}\begin{pmatrix}u_k\\ v_k\end{pmatrix} = \begin{pmatrix}H_1 & H_2\\ -H_2^* & -H_1^*\end{pmatrix}\begin{pmatrix}u_k\\ v_k\end{pmatrix}, \tag{2}$$

where $H_1=\hat{p}^2/2+g|\psi|^2-\mu+gQ|\psi|^2Q+K(\cos\theta)\delta_t(T)$, $H_2=gQ\psi^2Q^*$, μ is the chemical potential of the ground state, ψ is the ground state of the GP equation, and the projection operators Q are given by $Q=1-|\psi\rangle\langle\psi|$.

The number of noncondensed atoms describes the deviation from the condensate wave function and its growth rate characterizes the stability of the condensate. If the motion of the condensate is stable, the number of noncondensed atoms grows at most polynomially with time and no fast depletion of the condensate is expected. In contrast, if the motion of the condensate is chaotic, the number of noncondensed atoms diverges exponentially with time and the condensate may be destroyed in a short time. Therefore the rate of growth of the noncondensed atoms number is similar to the Lyapunov exponent for the divergence of trajectories in phase space for classical systems [6].

III. WEAK INTERACTIONS: ANTIRESONANCE AND QUANTUM BEATING

In this section, we focus our attention on the case of quantum antiresonance, and show how weak interactions between atoms modify the dynamics of the condensate. Quantum antiresonance is a single-particle phenomenon characterized by periodic recurrence between two different states, and its dynamics may be described by Eq. (1) with parameters $g=0$ and $T=2\pi$ [3].

A. Quantum beating

In a noninteracting gas, the energy of each particle oscillates between two values because of the periodic recurrence of the quantum states. In the presence of interactions, single-particle energy loses its meaning and we may evaluate the mean energy of each particle

$$E(t) = \int_0^{2\pi} d\theta\psi^*\left(-\frac{1}{2}\frac{\partial^2}{\partial\theta^2} + \frac{1}{2}g|\psi|^2\right)\psi. \tag{3}$$

To determine the evolution of the energy, we numerically integrate Eq. (1) over a time span of 100 kicks, using a split-operator method [22], with the initial wave function ψ being the ground state $\psi(\theta,0)=1/\sqrt{2\pi}$. After each kick, the energy $E(t)$ is calculated and plotted as shown in Fig. 1.

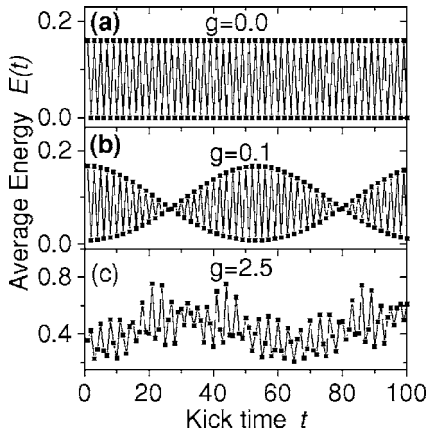

FIG. 1. Plots of average energy $E(t)$ versus the number of kicks t for three values of g. The kick strength $K=0.8$.

In the case of noninteraction [Fig. 1(a), $g=0$], we see that the energy $E(t)$ oscillates between two values and the oscillation period is $2T$, indicating the periodic recurrence between two states (antiresonance).

The energy oscillation with weak interaction ($g=0.1$) in Fig. 1(b) shows a remarkable difference from that for the noninteraction case. We see that the amplitude of the oscillation decreases gradually to zero and then revives, similar to the phenomenon of beating in classical waves. Clearly, it is the interactions between atoms in BEC that modulate the energy oscillation and produce the phenomena of *quantum beating*. As we know from classical waves, there must be two frequencies, *oscillation* and *beat*, to create a beating. These two frequencies are clearly seen in Fig. 2 that is obtained through Fourier transform of the energy evolutions in Fig. 1. For the noninteraction case [Fig. 2(a)], there is only the oscillation frequency $f_{osc}=0.5/T$, corresponding to one oscillation in two kicks. The interactions between atoms develop a new beat frequency f_{beat}, as well as modify the oscillation frequency f_{osc}, as shown in Fig. 2(b).

In Fig. 3, these two frequencies are plotted with respect to different interacting constant g and kick strength K. We see that both beat and oscillation frequencies vary nearly linearly

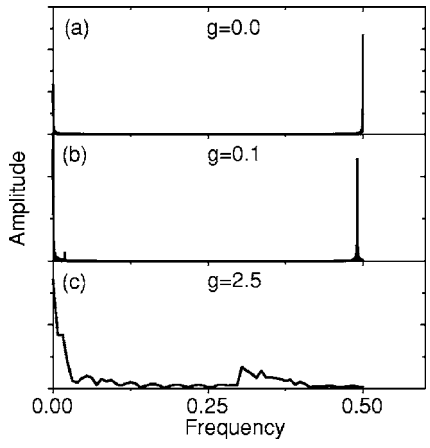

FIG. 2. Fourier transformation of the energy evolutions in Fig. 1. The unit for the frequency is $1/T$.

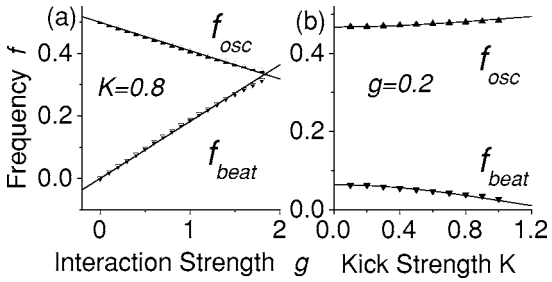

FIG. 3. Plots of beat and oscillation frequencies versus the interaction strength (a) and kick strength (b), where the scatters are the results from numerical simulation using the GP equation and lines from analytic expressions Eqs. (15) and (16).

with respect to the interaction strength g. More interestingly, the two frequencies satisfy a conservation relation

$$f_{osc} + f_{beat}/2 = 1/2. \tag{4}$$

For a strong interaction [Fig. 1(c)], i.e., $g \geqslant 1.96$, we find that the energy's evolution demonstrates an irregular pattern, clearly indicating the collapse of the quasiperiodic motion and the occurrence of instability. The corresponding Fourier transformation of the energy evolution [Fig. 2(c)] has no sharp peak. This transition to instability will be discussed in Sec. IV in details.

B. Spin model

The phenomena of quantum beating can be understood by considering a two-mode approximation [23] to the GP equation. In this approximation, condensed atoms can only effectively populate the two lowest second quantized energy modes. The validity of this two-mode model is justified by the following facts which are observed in the numerical simulation. First, the total energy of the condensate is quite small so that we can neglect the population at high-energy modes and keep only the states with quantized momentums 0 and ±1. Second, the total momentum of the condensate is conserved during the evolution. Therefore the populations of the states with momentum ±1 are same if the initial momentum of the condensate is zero (the ground state).

Here we consider a quantum approach of this two-mode model, which yields an effective spin Hamiltonian in the mean-field approximation. By considering the conservation of parity we may write the Boson creation operator for the condensate as

$$\hat{\psi}^\dagger = \frac{1}{\sqrt{2\pi}}(\hat{a}^\dagger + 2\hat{b}^\dagger \cos\theta), \tag{5}$$

where $\hat{a}^\dagger$ and $\hat{b}^\dagger$ are the creation operators for the ground state and the first excited states, satisfying the commutation relation $[\hat{a},\hat{a}^\dagger]=1$, $[\hat{b},\hat{b}^\dagger]=1$, and particle number conservation $\hat{a}^\dagger\hat{a}+\hat{b}^\dagger\hat{b}=N$.

Substituting Eq. (5) into the many-body Hamiltonian of the system

$$\hat{H} = \int_0^{2\pi} d\theta \left[\hat{\psi}^\dagger \left(-\frac{1}{2}\frac{\partial^2}{\partial\theta^2} \right) \hat{\psi} + \frac{g}{2N} \hat{\psi}^\dagger \hat{\psi}^\dagger \hat{\psi}\hat{\psi} + \hat{\psi}^\dagger (K(\cos\theta)\delta_T(t))\hat{\psi} \right], \tag{6}$$

we obtain a quantized two-mode Hamiltonian

$$\hat{H} = -\frac{1}{2}\hat{L}_z + \frac{g}{4\pi N}\left(4\hat{L}_x^2 - \frac{1}{2}(N-1)\hat{L}_z + \frac{1}{2}\hat{L}_z^2 \right) + \sqrt{2}K\hat{L}_x\delta_T(t) \tag{7}$$

in terms of the Bloch representation by defining the angular momentum operators,

$$\hat{L}_x = \frac{\hat{a}^\dagger\hat{b} + \hat{a}\hat{b}^\dagger}{2},$$

$$\hat{L}_y = \frac{\hat{a}^\dagger\hat{b} - \hat{a}\hat{b}^\dagger}{2i},$$

$$\hat{L}_z = \frac{\hat{a}^\dagger\hat{a} - \hat{b}^\dagger\hat{b}}{2}, \tag{8}$$

where we have discarded all c-number terms.

The Heisenberg equations of motion for the three angular momentum operators reads

$$\frac{d\hat{L}_x}{dt} = \frac{\hat{L}_y}{2} + \frac{g(N-1)}{4N}\hat{L}_y - \frac{g}{8\pi N}\{\hat{L}_y, \hat{L}_z\},$$

$$\frac{d\hat{L}_y}{dt} = -\frac{\hat{L}_x}{2} - \frac{g(N-1)}{8\pi N}\hat{L}_x - \frac{7g}{8\pi N}\{\hat{L}_z, \hat{L}_x\} - \sqrt{2}K\hat{L}_z\delta_T(t),$$

$$\frac{d\hat{L}_z}{dt} = \frac{g}{\pi N}\{\hat{L}_y, \hat{L}_x\} + \sqrt{2}K\hat{L}_y\delta_T(t), \tag{9}$$

where $\{\hat{L}_i, \hat{L}_j\} = \hat{L}_i\hat{L}_j + \hat{L}_j\hat{L}_i$.

The mean-field equations for the first-order expectation values $\langle\hat{L}_i\rangle$ of the angular momentum operators are obtained by approximating second-order expectation values $\langle\hat{L}_i\hat{L}_j\rangle$ as products of $\langle\hat{L}_i\rangle$ and $\langle\hat{L}_j\rangle$, that is, $\langle\hat{L}_i\hat{L}_j\rangle = \langle\hat{L}_i\rangle\langle\hat{L}_j\rangle$ [24]. Defining the single-particle Bloch vector

$$\vec{S} = (S_x, S_y, S_z) = \frac{2}{N}(\langle\hat{L}_x\rangle, \langle\hat{L}_y\rangle, \langle\hat{L}_z\rangle), \tag{10}$$

we obtain the nonlinear Bloch equations

$$\dot{S}_x = \left(\frac{1}{2} + \frac{g}{8\pi} - \frac{g}{8\pi}S_z \right) S_y,$$

$$\dot{S}_y = \left(-\frac{1}{2} - \frac{g}{8\pi} - \frac{7g}{8\pi}S_z \right) S_x - \sqrt{2}KS_z\delta_T(t),$$

$$\dot{S}_z = \frac{g}{\pi}S_yS_x + \sqrt{2}KS_y\delta_T(t), \tag{11}$$

where we have used $N \gg 1$. The mean-field Hamiltonian in the spin representation reads

$$\mathcal{H} = -\frac{S_z}{2} + \frac{g}{2\pi}\left(S_x^2 - \frac{S_z}{4} + \frac{S_z^2}{8} \right) + \sqrt{2}KS_x\delta_t(T). \tag{12}$$

From the definition of the Bloch vector, we see that S_z corresponds to the population difference and $-\arctan(S_y/S_x)$ corresponds to the relative phase α between the two modes. This Hamiltonian is similar to a kicked top model [25], but here the evolution between two kicks is more complicated.

With the spin model, we can readily study the dynamics of the system. For the noninteraction case ($g=0$), The Bloch equations (11) become

$$\dot{S}_x = \frac{1}{2}S_y,$$

$$\dot{S}_y = -\frac{1}{2}S_x - \sqrt{2}KS_z\delta_T(t),$$

$$\dot{S}_z = \sqrt{2}KS_y\delta_T(t). \tag{13}$$

We see that the evolution between two consecutive kicks is simply an angle π rotation about the z axis, which yields the spin transformation $S_x \to -S_x$, $S_y \to -S_y$. The spin initially directing to north pole $[\vec{S} = (0,0,1)]$ stays there for time duration T, then the first kick rotates the spin by an angle $\sqrt{2}K$ about the x axis and now $\vec{S} = (0, -\sin(\sqrt{2}K), \cos(\sqrt{2}K))$. The following free evolution rotates the spin to $\vec{S} = (0, \sin(\sqrt{2}K), \cos(\sqrt{2}K))$. Then, the second kick will drive the spin back to north pole through another rotation of $\sqrt{2}K$ about the x axis. With this the spin's motion is two kick period recurrence and quantum antiresonance occurs.

The motion of the spin is more complicated with interactions. The spin components at $\hat{x}$ and $\hat{y}$ directions can be written as $S_x = \sqrt{1-S_z^2}\cos\alpha$ and $S_y = -\sqrt{1-S_z^2}\sin\alpha$ in terms of population difference S_z and relative phase α, which yields the relation

$$\dot{S}_x = \dot{\alpha}S_y - \frac{g}{\pi}S_zS_y\cos^2\alpha$$

during the free evolution. Comparing this equation with the Bloch equation (11), we obtain the equation of motion for the relative phase,

$$\dot{\alpha} = \frac{1}{2} + \frac{g}{8\pi} + \frac{g}{2\pi}\left(\cos 2\alpha + \frac{3}{4} \right) S_z. \tag{14}$$

We see the motion between two consecutive kicks is approximately described by a rotation of $\pi + g(1+3S_z)/4$ about the z axis. Compared with the noninteraction case, the mean-field interaction leads to an additional phase shift $g(1+3S_z)/4$. This phase shift results in a deviation of the spin from $S_x = 0$ plane at time $2T^-$, i.e., the moment just before the second kick. As a result, the second kick cannot drive the

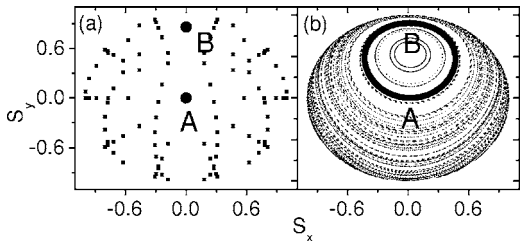

FIG. 4. Periodic stroboscopic plots of the projection of spin on the $S_z=0$ plane. The thick line and dots correspond to the orbits with initial spin $\vec{S}=(0,0,1)$. $K=0.8$ (a) $g=0.0$; (b) $g=0.1$.

spin back to its initial position and quantum antiresonance is absent. However, the phase shift will be accumulated in future evolution and the spin may reach the $S_x=0$ plane at a certain time mT^- (beat period) when the total accumulated phase shift is $\pi/2$. Then the next kick will drive the spin back to north pole by applying an angle $\sqrt{2}K$ rotation about the x axis.

The above picture is confirmed by our numerical solution of the spin Hamiltonian with the fourth-order Runge-Kutta method [26]. In Fig. 4, we plot the phase portraits of the spin evolution by choosing different initial conditions of the population difference S_z and relative phase α. Just after each kick three spin components S_i $(i=x,y,z)$ are determined and their projections on the $S_z=0$ plane are plotted. For the noninteraction case [Fig. 4(a)], we see that the motion of the spin is an oscillation between the north pole A and another point B, indicating the occurrence of quantum antiresonance. The interaction between atoms changes the phase portraits dramatically [Fig. 4(b)]. Around the north pole, a fixed point surrounded by periodic elliptic orbits appears. The two-point oscillation is shifted slowly and forms a continuous and closed orbit, representing the phenomenon of quantum beating.

In Fig. 5 we see that the relative phase at the moment just before the even kicks increases almost linearly and reaches 2π in a beat period. The slope of the increment reads, $\gamma_{RP}=[\alpha(4T^-)-\alpha(2T^-)]/2$, which can be deduced analytically. With this and through a lengthy deduction, we obtain an analytic expression for the beat frequency to first order in g,

$$f_{beat} \approx \frac{g}{4\pi}[1+3\cos(\sqrt{2}K)]. \tag{15}$$

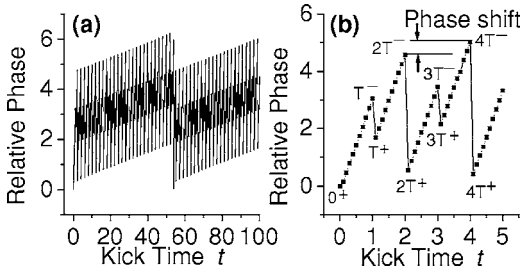

FIG. 5. (a) Plots of relative phase versus the number of kicks t, where $g=0.1$, $K=0.8$. (b) Schematic plot of the phase shift. $nT^{-(+)}$ represents the moment just before (after) the nth kick.

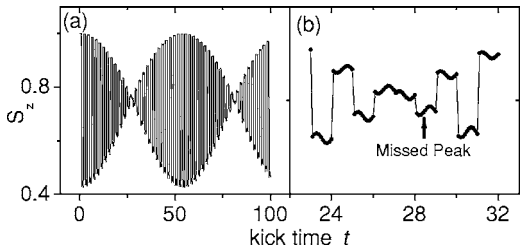

FIG. 6. (a) Plot of population difference versus the number of kicks t, where $g=0.1$, $K=0.8$. (b) Details of (a) at the middle of a beat period. The population difference decreases in two consecutive kicks.

In Fig. 6, we plot the evolution of population difference and the phenomenon of quantum beating is clearly seen in the spin model. Notice that there is a one-peak miss of the oscillation at the middle of one period because the population difference decreases in two consecutive kicks. Taking account of this missed peak, we obtain the oscillation frequency

$$f_{osc} \equiv \frac{N_{total}-N_{miss}}{2N_{total}} = \frac{1}{2} - \frac{1}{2}f_{beat}, \tag{16}$$

where N_{total} and N_{miss} are total and missed numbers of peaks, respectively.

The analytical expressions Eqs. (15) and (16) of the beat and oscillation frequencies are in very good agreement with the numerical results obtained from the GP equation, as shown in Fig. 3. Therefore the beating provides a method to measure interaction strength in an experiment.

C. Antiresonance with interactions

In the spin model, we see that it is the additional phase shift originating from weak interactions that destroys the two kick period recurrence of the antiresonance and leads to the phenomenon of quantum beating. Therefore we will still be able to observe the quantum antiresonance even in the presence of interactions if the additional phase shift may be compensated. Actually, the additional phase shift can be canceled by varying the kick period T so that the relative phase α only changes π between two consecutive kicks. Using Eq. (14), we find that the new kick period for antiresonance in the presence of interactions may be approximated as

$$T_{AR} \approx \frac{8\pi^2}{4\pi+g+3g\cos(\sqrt{2}K)}. \tag{17}$$

In Fig. 7, we plot the evolution of the average energy $E(t)$ with the new kick period T_{AR}. We see that the energy oscillates between two values and the oscillation period is $2T_{AR}$, clearly indicating the recovery of the antiresonance.

D. Decoherence due to thermal noise

In realistic experiments, the decoherence effects always exist. Generally, decoherence originates in the coupling to a bath of unobserved degree of freedom, or the interparticle entanglement process [27,28]. The main source of decoher-

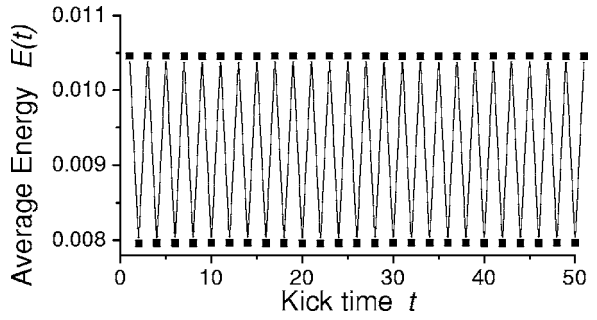

FIG. 7. Plots of average energy $E(t)$ versus the number of kicks t for $K=0.1$, $g=0.1$. T_{AR} is determined through Eq. (17).

ence in a BEC is the thermal cloud of particles surrounding the condensate. Thermal particles scattering off the condensate will cause phase diffusion at a rate Γ proportional to the thermal cloud temperature. For internal states not entangled with the condensate spatial state, Γ may be as low as 10^{-5} Hz under the coldest experimental condition [24], it may reach 2 Hz [29] or higher [30] depending on the practical experimental situation.

Modeling decoherence by fully include the quantum effects requires sophisticated theoretical studies that nontrivially include noncondensate atoms. In the experiments on BECs of dilute atomic gases trapped atoms are evaporatively cooled and they continuously exchange particles with their environment. Thus standard approaches of quantum optics for open systems involving quantum kinetic master equations seem especially natural for treating BECs [31],

$$\dot{\rho} = i[\rho, H] - \frac{\Gamma}{2}\sum_{l=a,b}[\hat{l}^{\dagger}\hat{l},[\hat{l}^{\dagger}\hat{l},\rho]], \tag{18}$$

where ρ is the N-body density operator.

Different approaches can be used to solve the Master equations [24], including (i) the mean-field treatment, (ii) the mean-field solution plus first-order quantum fluctuation, and (iii) the exact quantum solution. For our case of antiresonance and beating the mean-field solutions are stable so that the quantum breaking time is expected to be long enough ($\sim N$). It implies that the mean-field solution will follow the exact quantum solution for a long time. So, we adopt the simple mean-field treatment in our simulation. From the mean-field viewpoint, the decoherence term in Eq. (18) introduces a Γ transversal relaxation term into the mean-field equations of motion,

$$\dot{S}_x = \left(\frac{1}{2} + \frac{g}{8\pi} - \frac{g}{8\pi}S_z\right)S_y - \Gamma S_x,$$

$$\dot{S}_y = \left(-\frac{1}{2} - \frac{g}{8\pi} - \frac{7g}{8\pi}S_z\right)S_x - \sqrt{2}KS_z\delta_T(t) - \Gamma S_y,$$

$$\dot{S}_z = \frac{g}{\pi}S_yS_x + \sqrt{2}KS_y\delta_T(t). \tag{19}$$

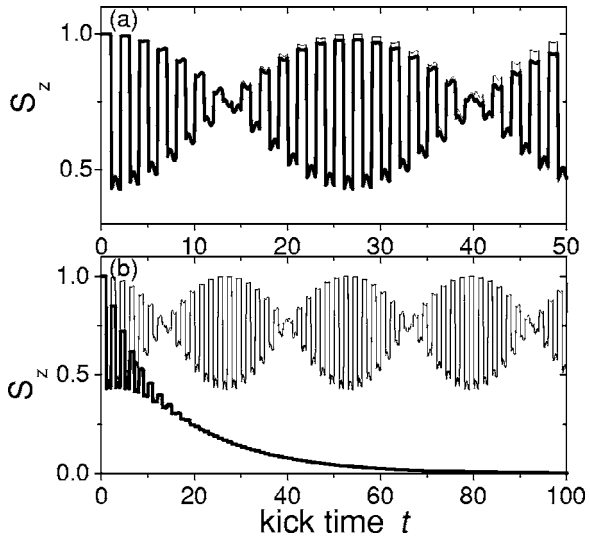

FIG. 8. Plots of population difference with respect to the number of kicks in the presence of decoherence. $K=0.8$, $g=0.2$. Thin lines correspond to $\Gamma=0$. Thick lines correspond to (a) $2\pi\Gamma/g=0.001$, (b) $2\pi\Gamma/g=1$.

In Fig. 8, we plot the evolution of the population difference S_z for different decoherence constant Γ. We see that the phenomenon of quantum beating is destroyed by strong thermal noise [Fig. 8(b)], while it survives in weak noise [Fig. 8(a)]. For large decoherence constant, the population difference S_z decays to 0 exponentially and the characteristic time is the just the decoherence time $\tau=1/\Gamma$. Therefore the decoherence time τ must be much larger than the beat period $2\pi/f_{beat}$ to observe the phenomenon of quantum beating, which yields

$$2\pi\Gamma/g \ll \frac{1}{4\pi}[1 + 3\cos(\sqrt{2}K)]. \tag{20}$$

In the case of $K=0.8$, Eq. (20) gives an estimation $2\pi\Gamma/g \ll 0.2$, which agrees with the numerical results shown in Fig. 8.

If we suppose our ring shape parameters of $r=5$ μm, $R=50$ μm [32] and use the typical data of ^{87}Rb, $a=5.7$ nm, the atom number is 10^4, the threshold rate approximates to a few tens of Hz, that is controllable in a practical situation.

IV. STRONG INTERACTIONS: TRANSITION TO INSTABILITY

A. Characterization of the instability: Bogoliubov excitation

Tuning the interaction strength still larger means enhancing further the nonlinearity of the system. From our general understanding of nonlinear systems, we expect that the solution will be driven towards chaos, in the sense of exponential sensitivity to initial condition and random evolution in the temporal domain. The latter character has been clearly displayed by the irregular pattern of the energy evolution in Fig. 1(c). On the other hand, the onset of instability (or chaotic motion) of the condensate is accompanied with the rapid proliferation of thermal particles. Within the formalism of

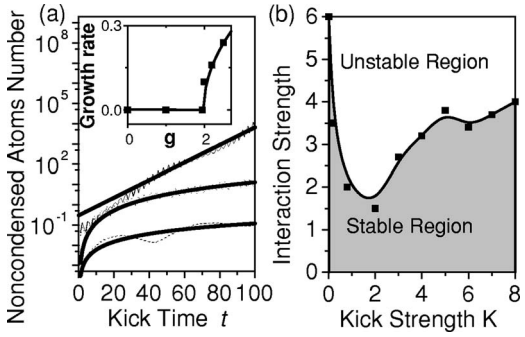

FIG. 9. (a) Semilog plot of the mean number of noncondensed atoms versus the number of kicks t. The thicker lines are fitting functions. $K=0.8$, $g=0.1$ (dashed line, fitting function $0.0003t^{1.3}$), $g=1.5$ (dotted line, fitting function $0.0011t^2$), $g=2.0$ [dash-dotted line, fitting function $0.32\exp(0.1t)$]. The inset shows the interaction dependence of the growth rate. The scatters are from numerical simulation and the solid line is the fitting function $0.33(g-1.96)^{1/2}$. (b) Phase diagram of the transition to instability.

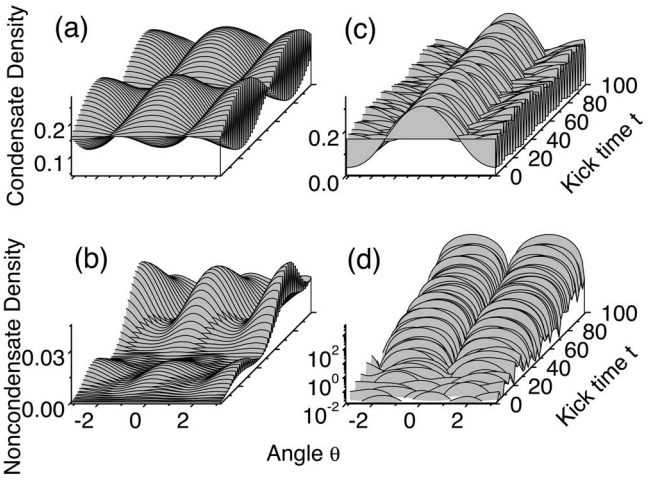

FIG. 10. Plots of condensate and noncondensate densities, where $K=0.8$. (a), (b) $g=0.1$; (c), (d) $g=2.0$.

Castin and Dum [11] described in Sec. II, the growth of the number of the noncondensed atom will be exponential, similar to the exponential divergence of nearby trajectories in phase space of classical system. The growth rate of the noncondensed atoms is similar to the Lyapunov exponent, turning from zero to nonzero as instability occurs.

We numerically integrate Bogoliubov equation (2) for the u_k, v_k pairs over a time span of 100 kicks, using a split operator method, parallel to numerical integration of the GP equation (1). The initial conditions

$$\begin{pmatrix} u_k(0) \\ v_k(0) \end{pmatrix} = \frac{1}{2}\begin{pmatrix} \zeta + \zeta^{-1} \\ \zeta - \zeta^{-1} \end{pmatrix} e^{ik\theta} \tag{21}$$

for initial ground-state wave function $\psi(\theta)=1/\sqrt{2\pi}$, are obtained by diagonalizing the linear operator in Eq. (2) [33], where $\zeta=[(k^2/2)/(k^2/2+2g|\psi|^2)]^{1/4}$.

After each kick the mean number of noncondensed atoms is calculated and plotted versus time in Fig. 9(a). We find that there exists a critical value for the interaction strength, i.e., $g_c=1.96$, above which the mean number of noncondensed atoms increases exponentially, indicating the instability of BEC. Below the critical point, the mean number of noncondensed atoms increases polynomially. As the nonlinear parameter crosses over the critical point, the growth rate turns from zero to nonzero, following a square-root law [inset in Fig. 9(a)]. This scaling law may be universal for Bogoliubov excitation as confirmed by recent experiments [12].

The critical value of the interaction strength depends on the kick strength. For very small kick strength, the critical interaction is expected to be large, because the ground state of the ring-shape BEC with repulsive interaction is dynamically stable [34]. For large kick strength, to induce chaos, the interaction strength must be large enough to compete with the external kick potential. So, in the parameter plane of (g,k), the boundary of instability shows a "U"-type curve [Fig. 9(b)].

Across the critical point, the density profiles of both condensed and noncondensed atoms change dramatically. In Fig. 10, we plot the temporal evolution of the density distributions of condensed atoms as well as noncondensed atoms. In the stable regime, the condensate density oscillates regularly with time and shows a clear beating pattern [Fig. 10(a)], whereas the density of the noncondensed atoms grows slowly and shows main peaks around $\theta=\pm\pi$ and 0, besides some small oscillations [Fig. 10(b)]. In the unstable regime, the temporal oscillation of the condensate density is irregular [Fig. 10(c)], whereas the density of noncondensed atoms grows explosively with the main concentration peaks at $\theta=\pm\pi/2$ where the gradient density of the condensed part is maximum [Fig. 10(d)]. Moreover, our numerical explorations show that the $\cos^2\theta$ mode [Fig. 10(b)] dominates the density distribution of the noncondensed atoms as the interaction strength is less than 1.8. Thereafter, the $\sin^2\theta$ mode grows while $\cos^2\theta$ mode decays, and finally $\sin^2\theta$ mode become dominating in the density distribution of noncondensed atoms above the transition point [Fig. 10(d)]. Since the density distribution can be measured in experiment, this effect can be used to identify the transition to instability.

B. Arnold diffusion

We have seen that strong interactions destroy the beating solution of the GP equation and the motion of the condensate becomes chaotic, characterized by exponential growth in the number of noncondensed atoms. The remaining question is how the motion of condensate is driven to chaos, that is, the route of the transition to instability.

The transition to chaos for the motion of the condensate can be clearly seen in the periodic stroboscopic plots of the trajectories for both two-mode approximation [Figs. 11(a)–11(d)] and four-mode approximation [Figs. 11(e) and 11(f); it is exact for the interaction region we consider in Fig. 11] to the original GP equation (1). The solution oscillates between two points A and B (point C is identical to A in the the spin model) for the noninteraction case, and forms a closed path in the phase space for the weak interaction [Fig. 11(a)]. Note that compared with the two-mode calculation, the effective interaction strength in the four-mode approxi-

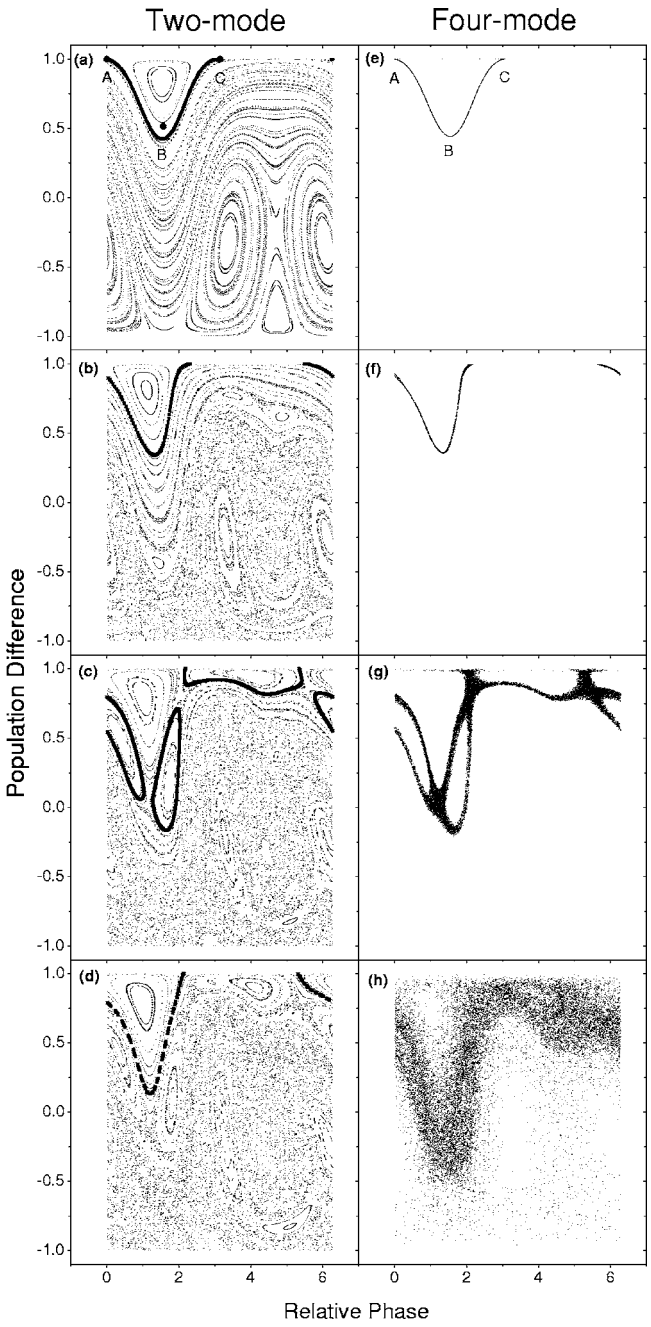

FIG. 11. Periodic stroboscopic plots of population difference with respect to the relative phase between the first two modes. $K=0.8$. (a)–(d) the two-mode model, where (a) $g=0.1$, circle dots corresponds to $g=0$; (b) $g=1.5$; (c) $g=1.9$; (d) $g=2.0$; The thicker line and larger dots on the phase portraits represent the trajectories with initial conditions $S_z=1$, $\alpha=0$. (e)–(h) the four-mode approximation. The portrait is the projection on the first two modes of the trajectory with initial condition $S_z=1$, $\alpha=0$. (e) $g=0.1$; (f) $g=1.6$; (g) $g=2.2$; (h) $g=2.5$.

mation is rescaled, to give the comparable pattern in the phase space.

With increasing interaction strength, the stable quasiperiodic orbits in Fig. 11(b) bifurcate into three closed loops [Fig. 11(c)] and chaos appears in the neighborhood of the hyperbolic fixed points. However, diffusion from one stochastic region to another are still blocked by KAM tori for the two-mode system. In Fig. 11(d), the trajectory with initial condition $S_z=1$, $\alpha=0$ is closer to the chaotic region.

The above discussion is based on two-mode approximation; actually, the solution is coupled with other modes of higher energy states. For small interaction, this coupling is negligible and the four-mode simulation gives the same results as seen in Figs. 11(a), 11(b), 11(e), and 11(f). For large interaction, this coupling is important and our system is essentially high dimensional ($d>2$). One important character of a high-dimensional dynamical system is that KAM tori (d dimension) cannot separate phase space ($2d$ dimension) and the whole chaotic region is interconnected. If a trajectory lies in a chaotic region it can circumvent KAM tori and diffuse to higher energy states through Arnold diffusion. This process is clearly demonstrated in Figs. 11(g) and 11(h). We see that the trajectory diffuses along the separatrix layers, circumvents the KAM tori, and finally spreads over whole phase space [Fig. 11(h), $g=2.5$]. We also calculate the diffusion coefficient

$$D_E = \frac{2}{J(J-1)} \sum_{m>n} \frac{|E_m - E_n|^2}{T(m-n)}, \tag{22}$$

where E_m is the energy after the mth kick, J is the total number of kicks. For $g=2.2$ and $g=2.5$, the diffusion rates are 7.2×10^{-11} and 1.5×10^{-9}, respectively.

Arnold diffusion allows the state to diffuse into higher energy states, which destroys the quasiperiodic motion of the quantum beating and leads to the transition to instability. As Arnold diffusion occurs, the motion of the condensate becomes unstable and the number of the noncondensed atoms grow exponentially, as we have seen in above discussion.

Arnold diffusion is a general property of the nonlinear Schrödinger equation in the presence of strong interactions. However, it may be hard to observe the whole process of Arnold diffusion in realistic BEC experiments because of the limited number of atoms (10^6). As Arnold diffusion occurs, the instability of the condensate leads to the exponential growth of thermal atoms which destroy the condensate, as well as invalidate the GP equation (1) in a short time; while the clear signature of the whole Arnold diffusion process may only be observed in a relatively long period. On the other hand, Arnold diffusion may be observed in the context of nonlinear optics, where the GP equation (1) describes the propagation of photons. The number of photons is very large and the interactions between them are very weak, therefore it is possible to have a long diffusion process without invalidating the GP equation (1).

C. Dynamical localized states

Although the above discussions have been focused on a periodic state of antiresonance, the transition to instability due to strong interactions also follows a similar path for a dynamically localized state. The only difference is that we start out with a quasiperiodic rather than a periodic motion in the absence of interaction. This means that it will generally be easier to induce instability but still requires a finite strength of interaction.

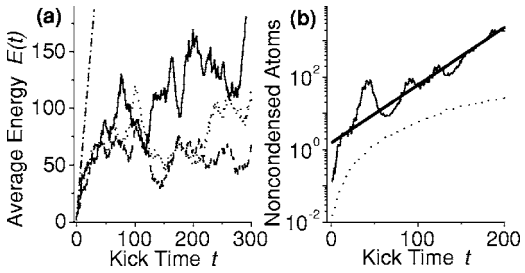

FIG. 12. Nonlinear effects on dynamically localized states. $K=5$, $T=1$. (a) Plots of average energy $E(t)$ versus the number of kicks t, where the dash-dotted line corresponds to the classical diffusion. $g=0$ (dash), $g=1$ (dot), $g=5$ (solid). (b) Semilog plot of the mean number of noncondensed atoms versus the number of kicks t. $g=1$ (dot), $g=5$ (solid).

In Fig. 12, we show the nonlinear effect on a dynamically localized state at $K=5$ and $T=1$. For weak interactions ($g=1$) the motion is quasiperiodic with slow growth in the number of noncondensed atoms. Strong interaction ($g=5$) destroys the quasiperiodic motion and leads to diffusive growth of energy, accompanied by exponential growth of noncondensed atoms that clearly indicates the instability of the BEC. Notice that the rate of growth in energy is much slower than the classical diffusion rate, which means that chaos brought back by interaction in this quantum system is still much weaker than pure classical chaos.

V. CONCLUSIONS

We have investigated the complex dynamics of a periodically kicked Bose-Einstein condensate that is considered as a nonlinear generalization of the quantum kicked rotor. We demonstrate the transition from the antiresonance to the quantum beating and then to instability with increasing many-body interactions, and reveal their underlying physical mechanism. The stable quasiperiodic motions for weak interactions, such as antiresonace and quantum beating, have been studied by mapping the nonlinear Schrödinger equation to a spin model. The transition to instability has been characterized using the growth rate of the noncondensed atoms number, which is polynomial for stable motion and exponential for chaotic motion of the condensate.

Finally, we emphasize that the results obtained in the paper are not limited to BEC and can be directly applied to other systems whose dynamics are governed by the nonlinear Schrödinger equation.

ACKNOWLEDGMENTS

We acknowledge support from the NSF and the R. A. Welch Foundation. M.G.R. acknowledges support from the Sid W. Richardson Foundation. J.L. was supported by the NSF of China (10474008), National Fundamental Research Programme of China under Grant No. 2005CB3724503, and the National High Technology Research and Development Program of China (863 Program) international cooperation program under Grant No. 2004AA1Z1220.

[1] L. E. Reichl, *The Transition to Chaos In Conservative Classical Systems: Quantum Manifestations* (Springer-Verlag, New York, 1992).

[2] G. Casati, B. V. Chirikov, J. Ford, and F. M. Izrailev, Lect. Notes Phys. **93**, 334 (1979); B. V. Chirikov, Phys. Rep. **52**, 263 (1979); F. M. Izrailev, *ibid.* **196**, 299 (1990).

[3] F. M. Izrailev and D. L. Shepelyansky, Sov. Phys. Dokl. **24**, 996 (1979); Theor. Math. Phys. **43**, 553 (1980); I. Dana, E. Eisenberg, and N. Shnerb, Phys. Rev. Lett. **74**, 686 (1995).

[4] F. L. Moore, J. C. Robinson, C. F. Bharucha, Bala Sundaram, and M. G. Raizen, Phys. Rev. Lett. **75**, 4598 (1995); W. H. Oskay, D. A. Steck, V. Milner, B. G. Klappauf, and M. G. Raizen, Opt. Commun. **179**, 137 (2000); M. B. d'Arcy, R. M. Godun, M. K. Oberthaler, D. Cassettari, and G. S. Summy, Phys. Rev. Lett. **87**, 074102 (2001).

[5] F. Benvenuto, G. Casati, A. S. Pikovsky, and D. L. Shepelyansky, Phys. Rev. A **44**, R3423 (1991); D. L. Shepelyansky, Phys. Rev. Lett. **70**, 1787 (1993).

[6] S. A. Gardiner, D. Jaksch, R. Dum, J. I. Cirac, and P. Zoller, Phys. Rev. A **62**, 023612 (2000); R. Artuso and L. Rebuzzini, Phys. Rev. E **66**, 017203 (2002).

[7] M. H. Anderson, J. R. Ensher, M. R. Matthews, C. E. Wieman, and E. A. Cornell, Science **269**, 198 (1995); C. C. Bradley, C. A. Sackett, J. J. Tollett, and R. G. Hulet, Phys. Rev. Lett. **75**, 1687 (1995); J. H. E. Cartwright, M. Feingold, and O. Piro, *ibid.* **75**, 3669 (1995).

[8] F. Dalfovo, S. Giorgini, L. P. Pitaevskii, and S. Stringari, Rev. Mod. Phys. **71**, 463 (1999); A. J. Leggett, *ibid.* **73**, 307 (1999).

[9] R. W. Boyd, *Nonlinear Optics* (Academic Press, San Diego, 1992).

[10] A. Vardi and J. R. Anglin, Phys. Rev. Lett. **86**, 568 (2001); G. P. Berman, A. Smerzi, and A. R. Bishop, *ibid.* **88**, 120402 (2002).

[11] Y. Castin and R. Dum, Phys. Rev. A **57**, 3008 (1998); Phys. Rev. Lett. **79**, 3553 (1997); Ph. Nozières and D. Pines, *The Theory of Quantum Liquids* (Addison-Wesley, Reading, MA, 1990) Vol. II.

[12] J. K. Chin, J. M. Vogels, and W. Ketterle, Phys. Rev. Lett. **90**, 160405 (2003).

[13] C. Zhang, J. Liu, M. G. Raizen, and Q. Niu, Phys. Rev. Lett. **92**, 054101 (2004).

[14] B. Hu, B. Li, J. Liu, and J. Zhou, Phys. Rev. E **58**, 1743 (1998); B. Hu, B. Li, J. Liu, and Y. Gu, Phys. Rev. Lett. **82**, 4224 (1999).

[15] V. I. Arnol'd, Sov. Math. Dokl. **5**, 581 (1964); K. Kaneko and R. J. Bagley, Phys. Lett. **110A**, 435 (1985); A. J. Lichtenberg and B. P. Wood, Phys. Rev. A **39**, 2153 (1989); B. P. Wood, A. J. Lichtenberg, and M. A. Lieberman, *ibid.* **42**, 5885 (1990); D. M. Leitner and P. G. Wolynes, Phys. Rev. Lett. **79**, 55 (1997); V. Ya. Demikhovskii, F. M. Izrailev, and A. I. Malyshev, *ibid.* **88**, 154101 (2002).

[16] T. Hogg and B. A. Huberman, Phys. Rev. Lett. **48**, 711 (1982); S. Fishman, D. R. Grempel, and R. E. Prange, *ibid.* **49**, 509 (1982).
[17] L. D. Carr, C. W. Clark, and W. P. Reinhardt, Phys. Rev. A **62**, 063610 (2000); G. M. Kavoulakis, *ibid.* **67**, 011601(R) (2003); R. Kanamoto, H. Saito, and M. Ueda, *ibid.* **67**, 013608 (2003).
[18] V. Milner, J. L. Hanssen, W. C. Campbell, and M. G. Raizen, Phys. Rev. Lett. **86**, 1514 (2001); N. Friedman, A. Kaplan, D. Carasso, and N. Davidson, *ibid.* **86**, 1518 (2001).
[19] E. M. Wright, J. Arlt, and K. Dholakia, Phys. Rev. A **63**, 013608 (2000).
[20] B. Mieck and R. Graham, cond-mat/0411648.
[21] J. M. Gerton, D. Strekalov, I. Prodan, and R. G. Hulet, Nature (London) **408**, 692 (2000); E. A. Donley, N. R. Claussen, S. L. Cornish, J. L. Roberts, E. A. Cornell, and C. E. Wieman, *ibid.* **412**, 295 (2001).
[22] A. D. Bandrauk and H. Shen, J. Phys. A **27**, 7147 (1994).
[23] Jie Liu, Biao Wu, and Qian Niu, Phys. Rev. Lett. **90**, 170404 (2003).
[24] J. R. Anglin and A. Vardi, Phys. Rev. A **64**, 013605 (2001).
[25] F. Haake, *Quantum Signature of Chaos* (Springer-Verlag, New York, 2000).
[26] W. H. Press *et al.*, *Numerical Recipes in C++* (Cambridge, New York, 2000).
[27] M. Schlosshauer, Rev. Mod. Phys. **76**, 1267 (2004).
[28] W. H. Zurek, Rev. Mod. Phys. **75**, 715 (2003).
[29] D. Jaksch, C. W. Gardiner, K. M. Gheri, and P. Zoller, Phys. Rev. A **58**, 1450 (1998).
[30] D. A. R. Dalvit, J. Dziarmaga, and W. H. Zurek, Phys. Rev. A **62**, 013607 (2000).
[31] D. Jaksch, C. W. Gardiner, and P. Zoller, Phys. Rev. A **56**, 575 (1997); J. Anglin, Phys. Rev. Lett. **79**, 6 (1997); J. Ruostekoski and D. F. Walls, Phys. Rev. A **58**, R50 (1998).
[32] T. P. Meyrath, F. Schreck, J. L. Hanssen, C.-S. Chuu, and M. G. Raizen, Phys. Rev. A **71**, 041604(R) (2005).
[33] Y. Castin, in *Coherent Atomic Matter Waves*, edited by R. Kaiser *et al.* (EDP Sciences and Springer-Verlag, New York, 2001).
[34] B. Wu and Q. Niu, Phys. Rev. A **64**, 061603(R) (2001); J. R. Anglin, *ibid.* **67**, 051601(R) (2003).